kcal mol^{-1} at zero temperature, corresponding to ~149.5 kcal mol^{-1} at 298 K (7). Although such a remarkable agreement can be partially fortuitous, the substantial accord established by our work between high-level ab initio calculations and mass spectrometric results in the O_3/O_3H^+ system is reassuring.

A preliminary survey of the gas phase chemistry of O_3H^+ has revealed several interesting aspects. In one of these, by allowing isolated O_3H^+ ions to react with methane, we observed the exothermic process

$$O_3H^+ + CH_4 \rightarrow CH_3^+ + H_2O + O_2 \quad (3)$$

where $\Delta H_3^\circ = -31 \pm 3$ kcal mol^{-1}. This is followed by the well-known addition process

$$CH_3^+ + CH_4 \rightarrow C_2H_5^+ + H_2 \quad (4)$$

The above sequence is the gas phase counterpart of the oligomerization of CH_4 observed by Olah and co-workers in cold solutions of O_3 in "magic acid" (HSO_3F-SbF_5); our ion cyclotron resonance results here substantiate their mechanistic hypothesis based on the intermediacy of O_3H^+ (2).

REFERENCES AND NOTES

1. G. Slomp and J. L. Johnson, *J. Am. Chem. Soc.* **80**, 915 (1958).
2. G. A. Olah, N. Yoneda, D. G. Parker, *ibid.* **98**, 5261 (1976).
3. N. Yoneda and G. A. Olah, *ibid.* **99**, 3113 (1977).
4. G. A. Olah, D. G. Parker, N. Yoneda, *Angew. Chem. Int. Ed. Engl.* **17**, 909 (1978).
5. M. Kausch and P. von R. Schleyer, *J. Comput. Chem.* **1**, 94 (1980).
6. K. B. Mathisen, O. Gropen, P. N. Skancke, U. Wahlgran, *Acta Chem. Scand.* **A37**, 817 (1983).
7. C. Meredith, G. E. Quelch, H. F. Schaefer III, *J. Am. Chem. Soc.* **113**, 1186 (1991).
8. I. I. Zakharov, O. I. Kolbasina, T. N. Semenyuk, N. Tyupalo, G. M. Zhidomirov, *Zh. Strukt. Khim.* **34**, 28 (1993).
9. F. Cacace, F. Grandinetti, F. Pepi, *Angew. Chem. Int. Ed. Engl.* **33**, 123 (1994).
10. ———, *J. Phys. Chem.* **98**, 2713 (1994).
11. S. G. Lias *et al.*, *J. Phys. Chem. Ref. Data Suppl.* **17**, 1 (1988).
12. For recently reevaluated PA values, see J. E. Szulejko and T. B. McMahon, *J. Am. Chem. Soc.* **115**, 7839 (1993).
13. Hydrogen abstraction by O_3^+ from CH_4 could conceivably contribute to the formation of O_3H^+. Ion cyclotron resonance experiments involving isolated O_3^+ ions have shown that the process is too slow in comparison with reaction 1 to contribute to the formation of O_3H^+.
14. Despite the careful choice of the experimental conditions, extensive decomposition (more than 90%) of O_3 occurs before the ion source of the spectrometer is entered.
15. T. Su and M. T. Bowers, in *Gas Phase Ion Chemistry*, M. T. Bowers, Ed. (Academic Press, New York, 1979), vol. 1, chap. 3.
16. The efficiency can be depressed if proton transfer is nearly thermoneutral or if hindered bases are involved (15) [H. Bücker and H.-F. Grützmacher, *Int. J. Mass Spectrom. Ion Processes* **109**, 95 (1991)].

17. Financial support from Ministero dell'Università e della Ricerca Scientifica e Tecnologica (MURST) and from Consiglio Nazionale delle Ricerche (CNR) is gratefully acknowledged. F. Angelelli performed the ion cyclotron resonance experiments with customary skill.

2 March 1994; accepted 22 April 1994

The Abundance of Heavy Elements in Interstellar Gas

Jason A. Cardelli

The Goddard high-resolution spectrograph aboard the Hubble Space Telescope has been used to produce interstellar abundance measures of gallium, germanium, arsenic, krypton, tin, thallium, and lead, the heaviest elements detected in interstellar gas. These heavy elements arise from stellar nuclear processes (slow- and rapid-process neutron capture) that are different from those that produce zinc and the lighter elements previously observed. These data allow investigators to study how the heavy elements chemically interact with interstellar dust and to compare interstellar heavy element abundances in the current galactic epoch to those present at the time of the formation of the solar system. For example, the data indicate that the abundance of atoms in interstellar dust cannot be explained by simple condensation models alone and must be heavily influenced by chemistry in the interstellar medium. Also, the data for some elements suggest that their true galactic cosmic abundances may be different from the "fossil" abundances incorporated into the solar system 4.6 billion years ago.

The abundances of atomic elements in the galaxy are expected, on average, to reflect the history of galactic chemical evolution produced through a wide range of stellar nuclear processes. The study of elemental abundances in the interstellar medium (ISM) through absorption line spectroscopy affords an opportunity to explore (i) the efficiency with which heavy elements produced by local events (for example, supernovae and evolving moderate to low mass stars) mix with the existing gas and (ii) the nature of the condensation of elements from the gas phase onto dust.

Of particular interest are atomic transitions that arise from elements in the dominant state of ionization in the ISM that are heavier than Zn (atomic number $Z = 30$), the heaviest element previously detected in the ISM gas (*1*, *2*). The solar system abundances of these elements, obtained from both the sun and meteorites (C1 chondrites) (*3*), are very low; even the strongest absorption lines are so weak that observing them requires the use of the moderate to high-resolution gratings and the high signal-to-noise (S/N) (>>100/1) capabilities of the Goddard high-resolution spectrograph (GHRS) (*4*–*6*) aboard the Hubble Space Telescope (HST). By exploiting these capabilities, the GHRS has been used to obtain interstellar absorption line data for Ga ($Z = 31$), Ge ($Z = 32$), As ($Z = 33$), Kr ($Z = 36$), Sn ($Z = 50$), Tl ($Z = 81$), and Pb ($Z = 82$) in the spectra of several background stars (*4*, *7*, *8*). However, the entire ensemble of elements has thus far only been observed toward ζ Ophiuchi, a bright O-star at a distance of about 200 pc.

These heavy elements are significant because they derive from nuclear processes [slow (*s*) and rapid (*r*) neutron capture onto lighter elements arising in a diverse range of stellar progenitors] that differ from those that produce Zn and the lighter elements (nuclear statistical equilibrium and lighter element burning occurring at high temperatures). Specifically, *s*-process nucleosynthesis arises whenever the time between successive neutron captures is much longer than the relevant beta decay time scale, whereas *r*-process nucleosynthesis arises from neutron capture on time scales of the order of 10^{-5} s (for example, supernovae). Consequently, a comparative study of heavy elements allows us to explore the possible effects of local chemical enrichment and mixing in the interstellar gas and the efficiency with which heavy elements are bound into interstellar dust. In addition, for some elements, these data represent the first abundance measurements outside of the solar system. Thus, these data can also provide the opportunity to probe the nature of the solar system abundances with respect to the possible influence of local chemical enrichment on the presolar nebula. This is particularly relevant considering that solar system abundances are commonly used as the cosmic reference standard in general abundance studies.

In the study of interstellar heavy element abundances, the critical atomic transitions arise from the ground state of atoms in their dominant ionization state, and the vast majority of these transitions corre-

Washburn Observatory, University of Wisconsin–Madison, 475 North Charter Street, Madison, WI 53706, USA.

spond to ultraviolet (UV) wavelengths attainable only from observations with orbiting satellites. Furthermore, the absorption lines produced by most of the heavy elements discussed here are expected to be very weak. For example, for the transitions of As, Tl, and Pb observed in the spectrum of ζ Oph, the central absorption depths are ≤1% of the continuum intensity (9). Consequently, the detection of these atomic transitions requires data of moderate-to-high resolution with S/N limits in excess of 200, capabilities that were not available before the launch of HST.

Although attaining such high-quality data in the UV with the GHRS is relatively straightforward, the presence of nonphoton noise (the result of scratches in the transmission window and granularity, blemishes, and nonuniformities in the photocathode) in the detector system of the GHRS instrument requires that considerable care be taken both in the planning of the observations and in the reduction of the data. We have used specific innovative observing strategies and reduction techniques (*10*) that allow us to independently solve for (and remove) the effects of the nonphoton noise portion of the spectrum. Use of these techniques results in data that are at or very near the expected photon noise limit [S/N = (total counts)$^{1/2}$]. In fact, the data obtainable with the GHRS are of such quality that the accuracy of measured abundances in many instances is limited only by the uncertainty in the atomic data.

Figure 1 shows the line profiles of Pb II (wavelength λ 1433.9 Å) and Kr I (λ 1235.8 Å) observed in the spectrum of ζ Oph. Also shown are the empirically derived continuum S/N values and the measured line equivalent widths, W_λ, defined as the area of the profile in wavelength space normalized by the continuum intensity in units of thousandths of an angstrom (mÅ). For very weak lines, W_λ is directly proportional to the number of absorbers per square centimeter along the path to the star. The data in Fig. 1 typify the general quality and range of line strengths of the heavy element data discussed here.

Table 1 lists the logarithm of $A_{X/H}$, the gas-phase abundance (ratio of the number of atoms of X to atoms of H) of the heavy elements observed toward ζ Oph on the standard log H = 12 scale. The abundances were derived from a direct integration of the observed weak line profiles based on use of the available transition oscillator strengths (*4, 11*). For some elements, data for several absorption lines were available. In the limit of very weak absorption lines, direct profile integration produces reliable abundances that do not require potentially uncertain corrections for the saturation

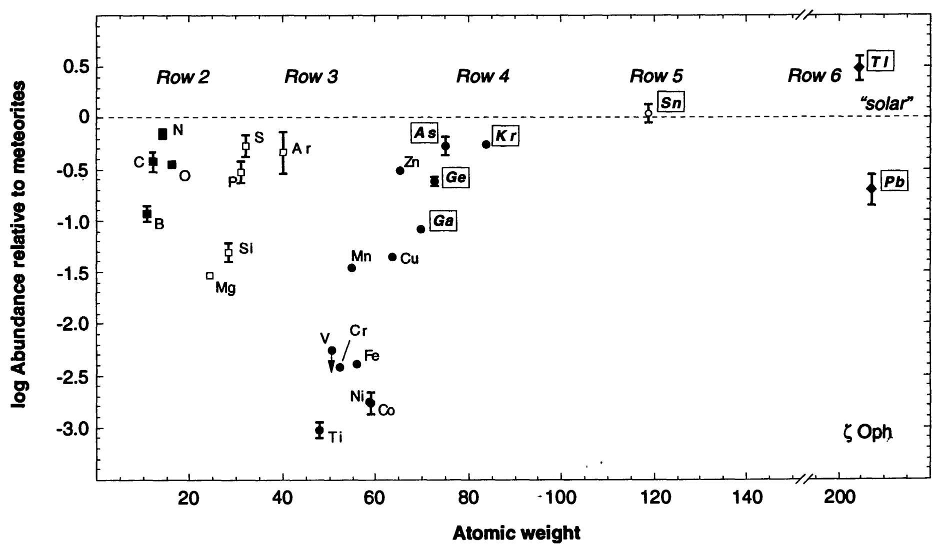

Fig. 2. The logarithm of the abundances of the heavy elements (boxed) observed toward ζ Oph (Table 1) relative to meteoritic (solar) abundances (*3*) plotted against mean atomic weight. For completeness we have also included data for the lighter elements. The specific rows in the periodic table in which these elements reside are also indicated and plotted with different symbols. The general deviation of different elements from the solar values is the result of their incorporation into dust.

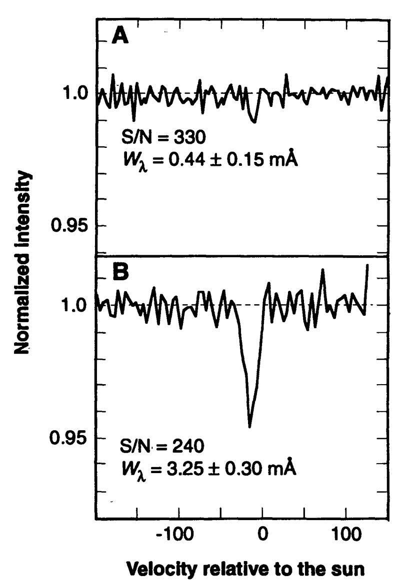

Fig. 1. Absorption lines of (**A**) Pb II λ 1433.9 Å and (**B**) Kr I λ 1235.8 Å observed in the spectrum of ζ Oph, plotted against the observed radial velocity (in kilometers per second) relative to the sun.

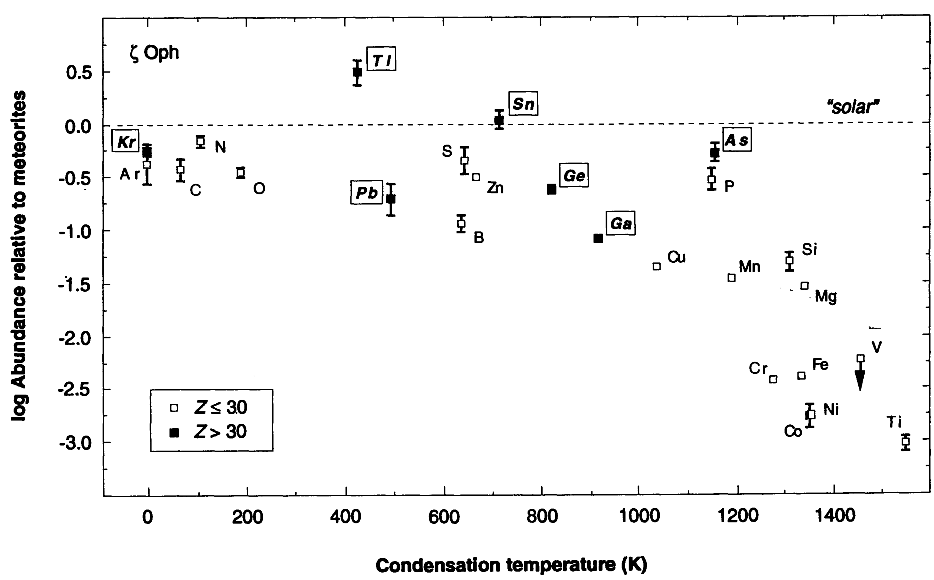

Fig. 3. The logarithm of the abundances of the heavy elements observed toward ζ Oph (Table 1) relative to meteoritic (solar) abundances (*3*) plotted against condensation temperature (*14*). For completeness we have also included data for the lighter elements. Although the overall trend is suggestive of a relation, the large degree of scatter indicates the strong domination of secondary processing in cold ISM gas.

generally associated with moderate-to-strong absorption lines (*12*). Because it is standard to compare abundances in the ISM with those of the solar system, the table also lists the heavy element abundances observed in the solar photosphere and meteorites (*3*).

Figure 2 is a plot of the logarithms of the ratios of the gas-phase abundances toward ζ Oph to those in the solar system, plotted against atomic weights. We have also included the observed abundances of the lighter elements, also obtained with the GHRS (except for Ar and Ti). For most of these lighter elements, the main difference between these data and previously published Copernicus satellite results (*13*) is higher precision, attributable mainly to higher S/N, resolution, and the availability of more reliable *f* values (*11*).

The observed deviation of interstellar gas-phase abundances from those in the solar system is generally thought to be the result of the formation of solid material (dust grains) in the ISM, and Fig. 2 shows that there are widely varying degrees of incorporation of elements (depletion) into dust. The observations of heavy element abundances now allow us to separate various rows of the periodic table. Within a given row, the observed deviations from solar values generally decrease from left to right, with very few exceptions. This behavior might be the result of a change in the relative chemical reactivity of elements with the dust related in part to the changing valence in unfilled shells. For example, the row 4 elements Ti ($Z = 22$) through Ni ($Z = 28$) are characterized by an unfilled 3*d* shell. For Ar and Kr, noble gases in their chemically inert (filled shell) neutral state in the cold ISM, the observed abundances are very near the solar values.

The data from Fig. 2 are also shown in Fig. 3, plotted against condensation temperature, defined as the temperature at which 50% of an element condenses into the solid phase. We calculated the values used in Fig. 3 assuming a cooling mixture represented by solar abundances at pressures of between 10^{-4} and 10^{-5} atm (*14*). Figure 3 suggests a general trend of decreasing gas-phase abundances (hence increasing incorporation into dust) with increasing condensation temperature. Although such a condensation sequence may apply on some level, there is strong evidence that significant interactions occur between dust grains themselves and also between the dust and gas in the cold ISM (*12, 15*). The data in Fig. 3 show that, on top of the overall trend, there is a huge amount of scatter (as large as a factor 50).

The addition of the heavy elements with relatively low condensation temperatures discussed here, along with GHRS data for B ($Z = 5$) (*16*), has provided an important test of the relation between depletion onto dust and condensation temperature in the previously undersampled low-to-moderate temperature domain. The scatter for these elements is also large (Fig. 3). In fact, if one considers the region in Fig. 3 between 400 and 1200 K, fully half of the total temperature range sampled, one sees little evidence for a link of depletion onto dust with condensation temperature.

We do not totally dismiss the general concept of a condensation temperature sequence. Condensation temperature is useful for displaying data like those in Fig. 3. Also, some form of a condensation sequence surely applies to the initial formation of dust in cooling stellar outflows, especially for elements with higher condensation temperatures. However, Fig. 3 indicates that the abundances of many elements vary considerably across different ISM environments where the notion of a condensation sequence does not apply. Consequently, condensation temperature alone is not a fundamental parameter for exploring element-to-element abundance variations.

Variations in the gas-phase abundance of a particular element may be caused either by intrinsic variations in the total abundance of the element, relative to H, among various sight lines, or by variations in the fraction of the element depleted onto dust. Data from the Copernicus satellite (*12, 15*) have shown that (i) the degree to which an element is depleted onto dust is strongly correlated with changes in parameters that characterize a sight line's physical conditions, like the mean sight line gas density (*12*), and (ii) as the depletion of one element changes, all depleted elements show changes in a similar sense (increase or decrease). In addition, the magnitude of the change in depletion is generally (although not always) larger for the more heavily depleted elements and smaller for more lightly depleted elements (*12, 17*).

The top panel in Fig. 4 shows the logarithm of the observed abundance of Mg, log (Mg/H), for sight lines taken from a Copernicus-based study (*18*), plotted against log $f(H_2)$, defined as the fractional abundance of hydrogen nuclei contained in molecular hydrogen, H_2. We choose this parameter because it is a measure of the change in physical conditions of the gas (the H_2 fraction measures the balance between H_2 grain surface formation and gas-phase chemical or photodestruction). The element Mg ($Z = 12$) shows a modest depletion from its solar value and a relatively smooth variation with $f(H_2)$ (Fig. 4). We expect that variations in the gas-phase Mg/H with $f(H_2)$ are related to depletion onto dust (*19*), because there is no reason why intrinsic elemental abundances should change as a result of variations in local cloud conditions. This mean variation of Mg/H with $f(H_2)$ is represented by the solid and dotted line fit through the data.

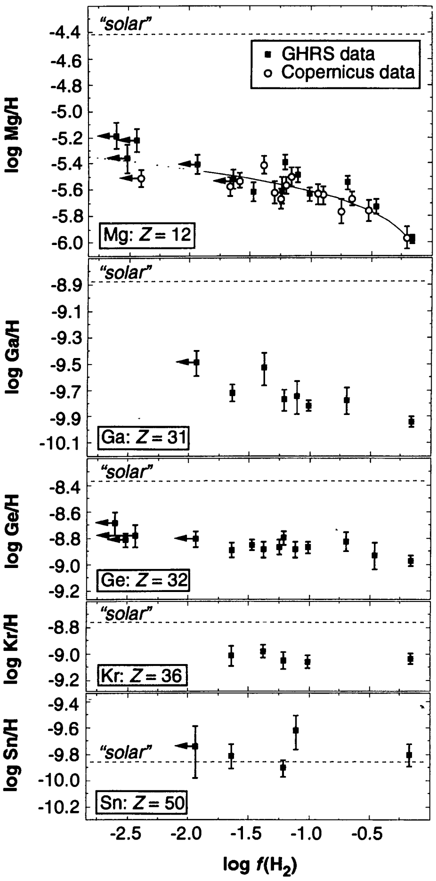

Fig. 4. The variation in the logarithm of the observed abundance, X/H, for the heavy elements Ga, Ge, Kr, and Sn as a function of log $f(H_2) \equiv \log [2H_2/(2H_2 + H\,I)]$, the fractional abundance of hydrogen nuclei contained in H_2. This parameter is an indicator of the change in the physical conditions of the cloud (that is, the balance between grain surface formation and photodestruction). Also shown is Mg/H for the same sight lines plus other values from Copernicus data. If the smooth variation of Mg/H with log $f(H_2)$ is argued to be the result of the effects of changing depletion onto dust, then it can be used as a guide to differentiate between the effects of dust and the effects of nucleosynthetic enrichment.

In Fig. 4 we also plot the observed abundances of the heavy elements Ga, Ge, Kr, and Sn for a number of different ISM sight lines (*8*) including the data for ζ Oph (Table 1). For each element we also plot the fit to the observed variation of Mg/H with $f(H_2)$. Although the data for Ga are limited, the decrease in abundance toward larger $f(H_2)$ as well as the average deficit from the solar value are quite similar to what is seen for Mg/H. For Ge, the element for which we have the most and best data, there is a perhaps a slight decrease in Ge/H with increasing $f(H_2)$, but it is only evident in the limit of large $f(H_2)$. The range of depletions among sight lines is typically smaller for elements with smaller average depletions from the solar value (*12, 17*). Although the current data for Kr and Sn are limited, neither appears to show any significant change with log $f(H_2)$ within the errors. Again, this seems reasonable for elements that exhibit small average depletions from the solar values.

We conclude that all of the abundance variations in Fig. 4 can probably be attributed to processes related to depletion onto dust. However, this same conclusion may not apply to the absolute abundances.

Figure 4 suggests that the proper reference abundances for Sn and Kr might not be our adopted solar system values. Krypton, which is neutral in the low-temperature ISM (ionization potential = 14.00 eV), is a noble gas ($4p^6$ outer shell) and consequently does not form chemical bonds. Because the van der Waals force is small, Kr is not prone to form significant mechanical bonds either. Consequently, we expect that Kr should not be depleted onto dust. However, to within the errors, all three sight lines for Kr are consistent with Kr/H being only about 60% of the solar value. We believe this discrepancy is not the result of problems in the observed abundances. For three of the sight lines in which Kr is observed, the abundance was derived from two separate transitions with both yielding self-consistent results. Also, experimental oscillator strengths for both transitions are available from two separate sources (*20, 21*) and are in very good agreement.

The solar reference abundance of Kr is based on a combination of the meteoritic abundance of one isotope, ^{84}Kr, and measured isotope ratios in the solar wind (*3*) from which the adopted abundance is obtained by fitting these data to adjacent elements assuming systematics of the *s*- and *r*-processes (*22*). Isotopes of Kr are also observed in cosmic rays, and the inferred abundance seems generally consistent with the solar value; however, the results are subject to the FIP (first ionization potential) correction (*23*). Consequently, it may very well be that the true "cosmic" abundance of Kr is more like that observed in the ISM than the currently adopted value for the solar system (*3*).

The data for Sn in Fig. 4 are intriguing in that they show no evidence for depletion onto dust at all, whereas all of the other group IV elements (C, Si, Ge, and Pb) are below their solar values by at least a factor of 3. Although it is possible that Sn resists being trapped on grain surfaces or is efficiently desorbed, its chemical properties are similar to those of Si or Ge (*24*). An increase of the reference abundance of Sn by a factor 2 to 3 would bring it more in line with the abundances relative to the solar values exhibited by the other group IV elements. The subsequent modest average depletion of Sn would not be inconsistent with the lack of observed variability with increasing $f(H_2)$. However, unlike Kr, for Sn we do not see an obvious justification for such a large discrepancy in the solar value. The meteoritic value is well determined, and, within the errors, the same value is found for the solar photosphere (*3*).

The gas-phase abundance measure for Tl, the fourth group III element (B, Al, Ga, and Tl) observed in the ISM, suggests an overabundance relative to the solar system. It is hardly possible that the oscillator strength of the observed line at λ 1321.7 Å is underestimated by a factor of 2 to 3, because there is relatively good agreement among the several available independent values (theoretical and experimental). Even if the observed gas-phase abundance of Tl were consistent with the solar value, all the other group III elements observed toward ζ Oph are below their solar values by at least a factor of 10 and so we would have a situation analogous to that of Sn.

We summarize the results presented here as follows. For the currently available data, it seems that variations in the observed gas-phase abundances of the heavy elements in several galactic directions can be explained by the effects of depletion of gas onto dust. However, this will be further explored through upcoming programs that will use the GHRS to observe Kr and Ge in additional galactic directions, and the data shown in Fig. 4 will be expanded to cover several more orders of magnitude in $f(H_2)$.

The current data for some heavy elements such as Kr strongly suggest that the solar system reference abundance is either appropriate or incorrect (*25*). For others, such as Sn and Tl, the lack of depletion (and possible evidence for an overabundance) might be linked to a general enrichment of these elements in the ISM today, relative to the "fossil" abundances appropriate to the solar system of 4.6 billion years ago. Considering that the time scales for nucleosynthesis and mass loss can vary significantly among stellar progenitors of widely varying mass, this would certainly seem a likely possibility. Future efforts should concentrate on these two elements. Both Sn (80% *s*-process) (*26*) and Tl (91% *s*-process) (*26*) are produced primarily by the *s*-process associated with the He shells of asymptotic giant branch (AGB) stars (the main *s*-process). A particularly useful comparison can be made to Kr because (i) Kr most likely does not deplete onto dust and (ii) Kr (76% *s*-process) (*26*) is produced mainly by the *s*-process associated with hydrostatic burning in massive stars (the "weak" *s*-process) (*27*).

Of all of the currently observed heavy elements, Pb, which is produced nearly exclusively by the *s*-process (99%) (*26*), may offer the best opportunity to search for the effects of local nucleosynthetic enrichment or incomplete mixing in the ISM, or both. Like Sn and Tl, Pb is also contributed to by the main *s*-process. However, it has been necessary to introduce a third *s*-process (the "strong" component) to account for the meteoritic abundance of ^{208}Pb, the most abundant isotope, near the termination of the *s*-process pathway. The site of this component is believed to be the He shell of low-mass metal-poor AGB stars (*28*).

The observed underabundance of Pb relative to the solar system could be the result of depletion onto dust. Given its relatively high mass, Pb may be especially prone to being trapped on grain surfaces. However, it has been suggested that the presence of evolving stars may have contributed to the

Table 1. Heavy element atomic data and measured abundances.

Species	Z	Weight	Isotopes†	T_c (K)‡	log Abundance*		
					ζ Oph§	Photosphere‖	Meteorites¶
Ga	31	69.7	2	918	2.06 (0.03)	2.88 (0.10)	3.13 (0.03)
Ge	32	72.6	5	825	3.02 (0.04)	3.41 (0.14)	3.63 (0.04)
As	33	74.9	1	1157	2.10 (0.09)		2.37 (0.05)
Kr	36	83.8	6	~0	2.97 (0.04)		3.23 (0.07)#
Sn	50	118.7	10	720	2.19 (0.09)	2.00 (0.30)	2.14 (0.04)
Tl	81	204.4	2	428	1.27 (0.12)	0.90 (0.20)	0.82 (0.04)
Pb	82	207.2	4	496	1.34 (0.15)	1.85 (0.05)	2.05 (0.03)

*Logarithm of the elemental abundances (the ratio of the number of atoms of X to atoms of H) on the standard log H = 12 scale, log ($A_{X/H}$) = log (X/H) + 12.00. The numbers in parentheses correspond to 1σ uncertainties. †Number of individual stable isotopes. ‡Condensation temperature, defined as the temperature at which 50% of the element condenses into the solid-state phase. We calculated these values assuming a cooling mixture represented by solar abundances at pressures of 10^{-4} to 10^{-5} atm (*14*). For the noble gas Kr, we assume $T_c \approx$ 0 K. §Heavy element abundances observed in the interstellar gas toward ζ Oph. ‖Abundances derived from the solar photosphere (*3*). ¶Abundances derived from meteorites (C1 chondrites) (*3*). #Kr data based on meteoritic measurement of the principal isotope, ^{84}Kr, along with measured solar wind isotope ratios from which the total abundance is derived by fitting these data to adjacent elements assuming systematics of the *s*- and *r*-processes.

presolar nebular environment (29). A more detailed study of the ISM abundance of Pb along the lines of Fig. 4 could help explore this interesting possibility further.

REFERENCES AND NOTES

1. A reported detection [M. Jura and W. H. Smith, *Astrophys. J.* **251**, L43 (1981)] of an optical line of Rb I ($Z = 37$), a trace ionization state in the ISM, was later shown to be incorrect (*2*). The original reported detection was attributed to a probable misidentification of a telluric feature.
2. S. R. Federman, C. Sneden, W. V. Schempp, W. H. Smith, *Astrophys. J.* **290**, L55 (1985).
3. E. Anders and N. Grevesse, *Geochim. Cosmochim. Acta* **53**, 197 (1989).
4. J. A. Cardelli, S. R. Federman, D. L. Lambert, C. E. Theodosiou, *Astrophys. J.* **416**, L41 (1993).
5. J. A. Cardelli, J. S. Mathis, D. C. Ebbets, B. D. Savage, *ibid.* **402**, L17 (1993).
6. J. A. Cardelli, U. J. Sofia, B. D. Savage, F. P. Keenan, P. L. Dufton, *ibid.* **420**, L29 (1994).
7. J. A. Cardelli, B. D. Savage, D. C. Ebbets, *ibid.* **383**, L23 (1991).
8. L. M. Hobbs, D. E. Welty, D. C. Morton, L. Spitzer, D. G. York, *ibid.* **411**, 750 (1993).
9. In the case of Pb, this corresponds to a sensitivity, relative to H_2, of 500 parts per trillion.
10. J. A. Cardelli and D. C. Ebbets, in *Attaining High Signal-to-Noise Data with the Goddard High Resolution Spectrograph* (Hubble Space Telescope Calibration Workshop, in press).
11. D. C. Morton, *Astrophys. J. Supp. Ser.* **77**, 119 (1991).
12. E. B. Jenkins, in *Interstellar Processes*, D. J. Hollenbach and H. A. Thronson, Eds. (Kluwer Academic, New York, 1987), pp. 533–559.
13. D. C. Morton, *Astrophys. J.* **197**, 85 (1975).
14. J. T. Wasson, *Meteorites: Their Record of the Early Solar System History* (Freeman, New York, 1985).
15. C. L. Joseph, *Astrophys. J.* **335**, 157 (1988).
16. S. R. Federman, Y. Sheffer, D. L. Lambert, R. L. Gilliland, *ibid.* **413**, L51 (1993).
17. B. D. Savage, J. A. Cardelli, U. J. Sofia, *ibid.* **401**, 706 (1992).
18. E. B. Jenkins, B. D. Savage, L. Spitzer, *ibid.* **301**, 355 (1986).
19. U. J. Sofia, J. A. Cardelli, B. D. Savage, *ibid.*, in press.
20. P. M. Griffen and J. W. Hutchenson, *J. Opt. Soc. Am.* **59**, 1607 (1969).
21. W. F. Chan, G. Cooper, X. Guo, G. R. Burton, C. E. Brion, *Phys. Rev. A* **46**, 149 (1992).
22. V. Trimble, *Astron. Astrophys. Rev.* **3**, 1 (1991).
23. C. J. Waddington, in *Origins of the Elements*, G. J. Mathews, Ed. (World, Singapore, 1988), p. 295.
24. M. J. Barlow, *Mon. Not. R. Astron. Soc.* **183**, 417 (1978).
25. This may also apply to some of the lighter elements. Observations of some young B-stars [D. R. Gies and D. L. Lambert, *Astrophys. J.* **387**, 673 (1992)] yield abundances of C and O that are below the solar values.
26. A. G. W. Cameron, *Astrophys. Space Sci.* **82**, 123 (1982).
27. C. M. Raiteri, R. Gallino, M. Busso, D. Neuberger, F. Kappler, *Astrophys. J.* **419**, 207 (1993).
28. R. Gallino, M. Busso, G. Picchio, C. M. Raiteri, in *Chemical and Dynamical Evolution of Galaxies*, F. Ferrini, J. Franco, F. Matteucci, Eds. (ETS Editrice, Pisa, 1990), p. 338.
29. U. Ott, *Nature* **364**, 25 (1993).

30. This research is based on observations obtained with the National Aeronautics and Space Administration (NASA)–European Space Agency Hubble Space Telescope through the Space Telescope Science Institute, which is operated by the Association of Universities for Research in Astronomy, Inc., under NASA contract NAS5-26555. I acknowledge useful discussions with D. L. Lambert, J. S. Mathis, and V. V. Smith. This research was supported under NASA's Long-Term Space Astrophysics Research Program (grant NAGW-2520).

3 March 1994; accepted 22 April 1994

On the Frequency-Locked Orbits of Two Particles in a Paul Trap

J. Hoffnagle* and R. G. Brewer

Calculations are presented that show frequency-locking to be a prominent phenomenon in the dynamics of two ions in a Paul trap, provided that damping is linear and small. The frequency-locked attractors that exist when dissipation is present correspond to stable, periodic orbits of the underlying Hamiltonian system, which appear to be infinite in number. The accuracy of the calculations is illustrated by comparing an orbit observed in a Paul trap for microspheres with the solution of the equations of motion.

Ion traps offer researchers the opportunity to study individual ions, which are nearly at rest and largely free from external perturbations, and these traps have important applications in spectroscopy, quantum optics, and metrology. When radiation pressure is used to cool trapped ions to millikelvin temperatures (*1*), unusual and interesting dynamical systems appear, Coulomb clusters, in which the electrostatic potential energy is large compared with the random thermal energy. The equations of motion of particles in a Paul trap are independent of the particle size, and several important dynamical phenomena, including transitions between ordered and chaotic motion, were first observed in an experiment on trapping of charged aluminium particles (*2*). But widespread interest in Coulomb cluster dynamics only followed the introduction of laser cooling and the observation in Paul traps of "ion crystals" (*3, 4*), for which the time-averaged confining force is just balanced by the ions' mutual electrostatic repulsion, yielding regular arrays in which the ions oscillate with the trap frequency about their average positions.

IBM Almaden Research Center, 650 Harry Road, San Jose, CA 95120, USA.

*To whom correspondence should be addressed.

Most work on trapped ion dynamics has focused on crystals, chaos, and the transition between these two states of motion (*5–7*). In particular, a transition from transient to stationary chaos was found when the trap parameters were varied (*8*). The crystal is not, however, the only regular solution of the equations of motion: in this report we show that frequency-locking (*5, 9*) is a prevalent feature of trapped ion dynamics and that, in general, the two-ion system is multistable, with many coexisting frequency-locked attractors. Although periodic orbits of two ions in a Paul trap were predicted several years ago, they were largely neglected, because only the crystal was observed in trapped ion experiments. We present the results of a systematic, numerical study of frequency-locking as the trap voltage and energy dissipation are varied. These results suggest that as the dissipation tends to zero, the number of frequency-locked orbits becomes infinite. It is notable that celestial mechanics, in which the nonlinear gravitational interaction has the same form as the electrostatic interaction between ions, is also rife with instances of frequency-locking (*10*); the orbital resonance by which Neptune and Pluto avoid close approaches, although their orbits cross, is particularly reminiscent of the ion trajectories.

We consider the simplest, nontrivial Coulomb cluster in a Paul trap—that of two ions. This is a particularly elementary problem in classical, nonlinear dynamics: two particles of charge e and mass m in a periodic electric potential

$$V(\mathbf{r},t) = (V_{DC} - V_{AC}\cos\Omega t)\frac{x^2 + y^2 - 2z^2}{2r_0^2} \quad (1)$$

where r_0 is a characteristic trap radius and V_{DC} and V_{AC} are the amplitudes of the applied potential with frequencies zero and Ω, respectively. The equations of motion separate into center-of-mass and relative components, the former obeying the same, linear Mathieu equation as does a single trapped particle. Therefore, we may restrict our attention to the relative coordinate $\mathbf{r}_{12}$, expressed in cylindrical coordinates as (r,ϕ,z). If dissipation is present, it damps the angular momentum L_ϕ, leaving two degrees of freedom. Introducing dimensionless units for time, $\tau = \Omega t/2$, and the electric potentials, $a = -8eV_{DC}/mr_0^2\Omega^2$, $q = 4eV_{AC}/mr_0^2\Omega^2$, and measuring length in units of $[\ell] = (2e^2/m\Omega^2)^{1/3}$, the equations of motion become coupled Mathieu-Coulomb equations: